# Supplementary information for

# Dual heterogeneous structures lead to ultrahigh strength and uniform ductility in a Co-Cr-Ni medium-entropy alloy

**Du et al.**

## Supplementary Note 1. Material Design

The deviation from the component of equi-atomic Ni-Co-Cr ternary alloy, namely, increasing Co content decreasing Ni content is to reduce the stacking fault energy (SFE) value of the FCC-structured matrix[1,2]. The Co-rich compositions are desirable owing to the following purposes (1) To intensify strain strengthening by forming high-density planar defects during the cold deformation process. (2) To suppress the recrystallization owing to the increased apparent activation energy of recrystallization[3]. (3) To promote the precipitation of $\gamma'$ phase *via* decreasing the solubility of Al and Ti in the $\gamma$ matrix[4]. In order to avoid the formation of brittle BCC phase only moderate contents of 3 at% Al and 3 at% Ti are added to precipitate the $\gamma'$ phase during the aging process.

**Supplementary Note 2. Estimation of the strengthening effect of the hierarchical precipitates**

Due to the near fully coherent relationship of FCC/$L1_2$ and ultrafine size, the precipitation strengthening $L1_2$ phase is substantially sheared by the gliding dislocations during the deformation. Hence, the strengthening effects of $L1_2$ phase $\Delta\sigma_P$ are from three contributing factors, i.e., coherency strengthening $\Delta\sigma_C$, modulus mismatch strengthening $\Delta\sigma_M$ and ordering strengthening $\Delta\sigma_O$. The $\Delta\sigma_C$ and $\Delta\sigma_M$ play a part prior to the shearing, while the last one makes a contribution during the shearing. As a result, the $\Delta\sigma_P$ is equal to the larger one of ($\Delta\sigma_C$ and $\Delta\sigma_M$) and $\Delta\sigma_O$, of which can be expressed as[5]:

$$\Delta\sigma_C = M\cdot\alpha_\varepsilon(G\cdot\varepsilon)^{3/2}\left(\frac{rf}{0.5Gb}\right)^{1/2} \quad (1)$$

$$\Delta\sigma_M = M\cdot 0.0055(\Delta G)^{3/2}\left(\frac{2f}{G}\right)^{1/2}\left(\frac{r}{b}\right)^{\frac{3m}{2}-1} \quad (2)$$

$$\Delta\sigma_O = 0.81M\frac{\gamma_{APB}}{2b}\left(\frac{3\pi f}{8}\right)^{1/2} \quad (3)$$

where the Taylor factor $M$=3.06, $\alpha_\varepsilon$=2.06 are constants for polycrystalline FCC structure and $G$=87 GPa is the shear modulus of the matrix (taken from the $(CoCrNi)_{94}Al_3Ti_3$ medium-entropy alloy[6]). $\Delta G$=87-77=10 GPa is the difference of shear modulus between FCC matrix and $L1_2$ precipitate[7]. $m$=0.85[8]. $\gamma_{APB}$ is the antiphase boundaries energy. As reported by literature about the Ni-based alloys, $\gamma_{APB}\approx 0.3$ J/m$^2$[9], $b=\frac{\sqrt{2}}{2}\alpha_{matrix}$=0.252 nm is the Burgers vector of the dislocation. $\varepsilon=2/3(\Delta\alpha/\alpha)$ is the misfit between matrix and precipitate, $r$ is the mean radius of precipitates and $f$ is the volume fraction of precipitates, where $n$ is the number density of the precipitates.

In this study, the size of $(Ni,Co)_3(Al,Ti)$ particles precipitated during the annealing process are larger than that formed during the aging process. So the overall precipitation strengthening effect contributed by these heterogeneous $(Ni,Co)_3(Al,Ti)$ particles can be divided into two parts, namely,

$$\Delta\sigma_P = \Delta\sigma_p^{I} + \Delta\sigma_p^{II} \quad (4)$$

$\Delta\sigma_p^I$ is contributed by $(Ni,Co)_3(Al,Ti)$ particles formed during the annealing process. Where $\varepsilon^{II}$=0.0056%, r=38.04 nm, $f$=13.25% (calculated from the APT results by using the level rule[10]), Using the above expressions, the values for $\Delta\sigma_C$, $\Delta\sigma_M$ and $\Delta\sigma_O$ are calculated as 1.45 MPa, 116.73 MPa and 585.22 MPa, respectively. As $\Delta\sigma_C + \Delta\sigma_M$ is far lower than $\Delta\sigma_O$, the $\Delta\sigma_p^I$ is derived from ordering strengthening.

Similarly, $\Delta\sigma_p^{II}$ is contributed by $(Ni,Co)_3(Al,Ti)$ particles formed during the aging process. $\varepsilon^I$=0.011%, $r$=2.07 nm and $f$=10.95%. So the values for $\Delta\sigma_C$, $\Delta\sigma_M$ and $\Delta\sigma_O$ are calculated as 0.85 MPa, 47.68 MPa and 530.14 MPa, respectively. As $\Delta\sigma_C + \Delta\sigma_M$ is far lower than $\Delta\sigma_O$, the $\Delta\sigma_p^I$ is also contributed by ordering strengthening.

Based on the above calculation, the precipitation strengthening effect of heterogeneous $L1_2$ phase is estimated to be about 1115 MPa.

**Supplementary Table 1. Compositions, structures of matrix, and tensile properties of the HEAs and MEAs studied previously.**

| Compositions | Matrix | $\sigma_y$ (MPa) | $\sigma_u$ (MPa) | $\varepsilon_{ue}$ (%) | Ref. |
|---|---|---|---|---|---|
| HfNbTaTiZr | BCC | 1202 | 1295 | 2 | 11 |
| | | 1303 | 1334 | 1.9 | |
| | | 1145 | 1262 | 9.7 | |
| | | 1600 | 1900 | 3 | 12 |
| | | 1520 | 1520 | 1.7 | |
| CoCrFeNiMn | FCC | 1400 | 1750 | 4 | 13 |
| | | 930 | 1030 | 2 | |
| FeNiCoCu | FCC | 1149 | 1402 | 5 | 14 |
| $(FeNiCoCu)_{86}Al_7Ti_7$ | FCC | 1477 | 1849 | 3.4 | |
| $Cr_{15}Fe_{20}Co_{35}Ni_{20}Mo_{10}$ | FCC | 1311 | 1410 | 10 | 15 |
| | | 1212 | 1360 | 14 | |
| | | 1028 | 1249 | 17 | |
| | | 879 | 1194 | 22 | |
| | | 799 | 1127 | 27 | |
| $(FeCoNiCr)_{94}Ti_2Al_4$ | FCC | 645 | 1094 | 30 | 16 |
| | | 1005 | 1273 | 15 | |
| TaHfZrTi | BCC | 1300 | 1500 | 2.4 | 17 |
| $Ni_{1.5}Co_{1.5}CrFeTi_{0.5}$ | FCC | 1308 | 1384 | 4.01 | 18 |
| $Fe_{25}Co_{25}Ni_{25}Al_{10}Ti_{15}$ | FCC | 1860 | 2520 | 5.2 | 19 |
| $Al_{0.5}Cr_{0.9}FeNi_{2.5}V_{0.2}$ | FCC | 1570 | 1763 | 10 | 20 |
| | | 1810 | 1905 | 9 | |
| $Fe_{49.5}Mn_{30}Co_{10}Cr_{10}C_{0.5}$ | FCC | 1300 | 1500 | 1.5 | 21 |
| $(FeCoNi)_{86}$-$Al_7Ti_7$ | FCC | 1028 | 1446 | 46.3 | 4 |

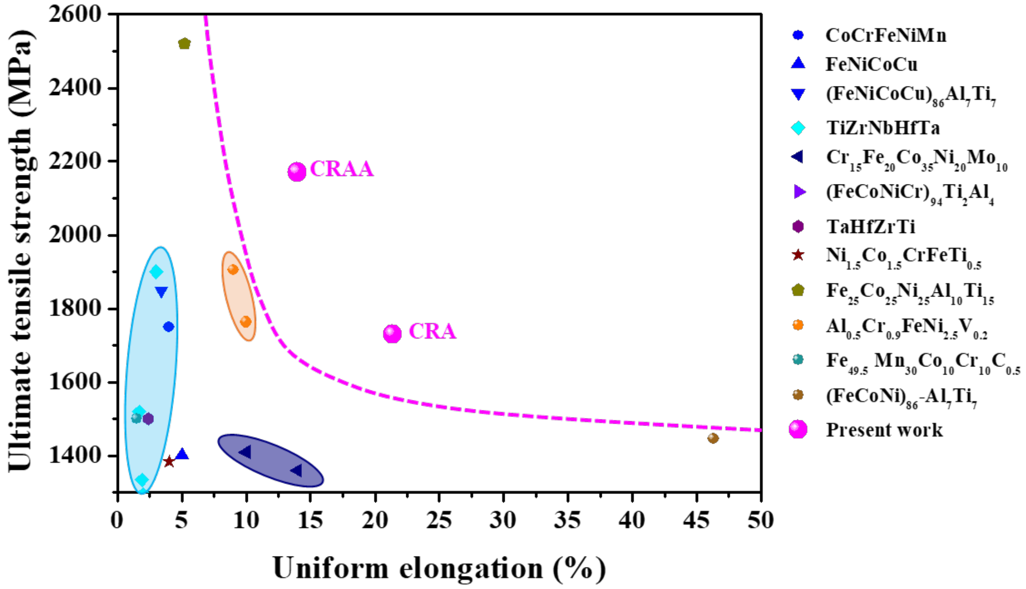


**Supplementary Figure 1. Comparison of our developed alloys and other high strength MEAs and HEAs.** Map of uniform elongation ($\varepsilon_{ue}$) versus ultimate tensile strength (UTS, $\sigma_u$) reveals the aged alloy achieves a combination of $\sigma_u$ and $\varepsilon_{ue}$ better than other high strength MEAs and HEAs using FCC or BCC as matrix. The data of the mechanical properties of these reported FCC-based materials are acquired from **Supplementary Table 1.**

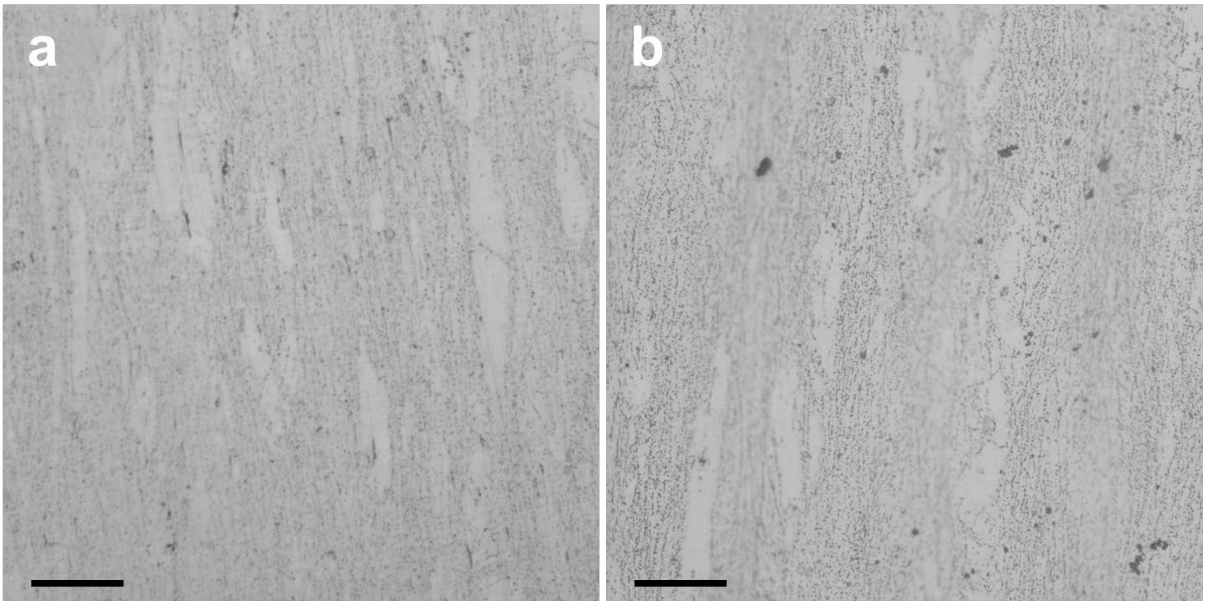


**Supplementary Figure 2. Microstructural characterization for the (a) CRA and (b) CRAA alloys,** revealing that many bands widely distributed in both CRA and CRAA alloys and surrounded by many fine grains. The scale bars in **(a)** and **(b)** are both 50 μm.

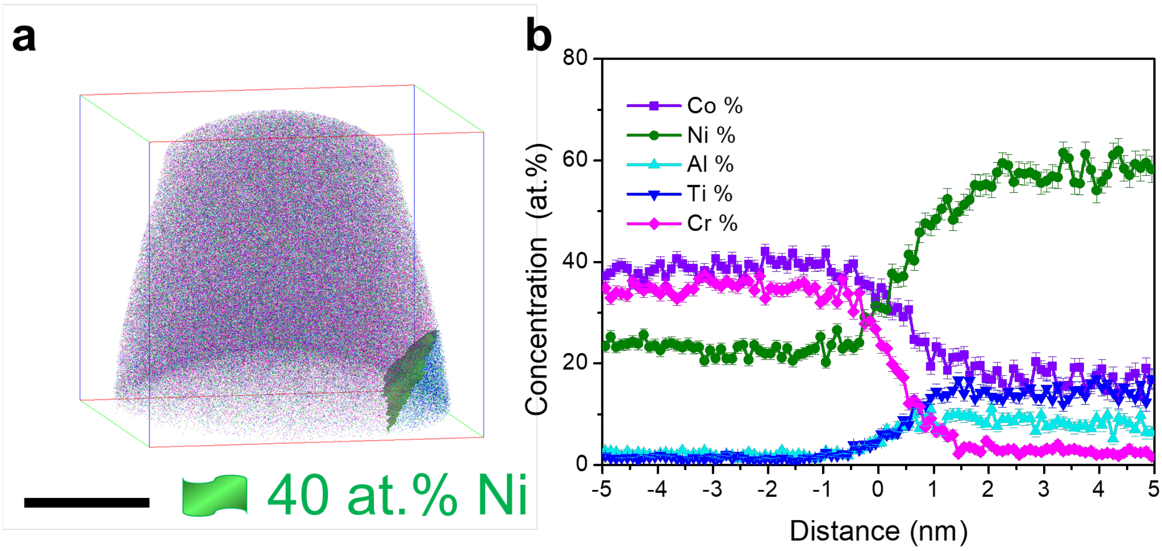


**Supplementary Figure 3. APT results of the CRA alloy. a**, the three-dimensional reconstruction of 40 at% Ni iso-concentration surfaces presenting the morphologies of a particle and matrix, respectively. Scale bar, 20 nm. **b**, one-dimensional concentration profile showing the element distributions from matrix to Ni-enriched particle. Error bars, s.d.

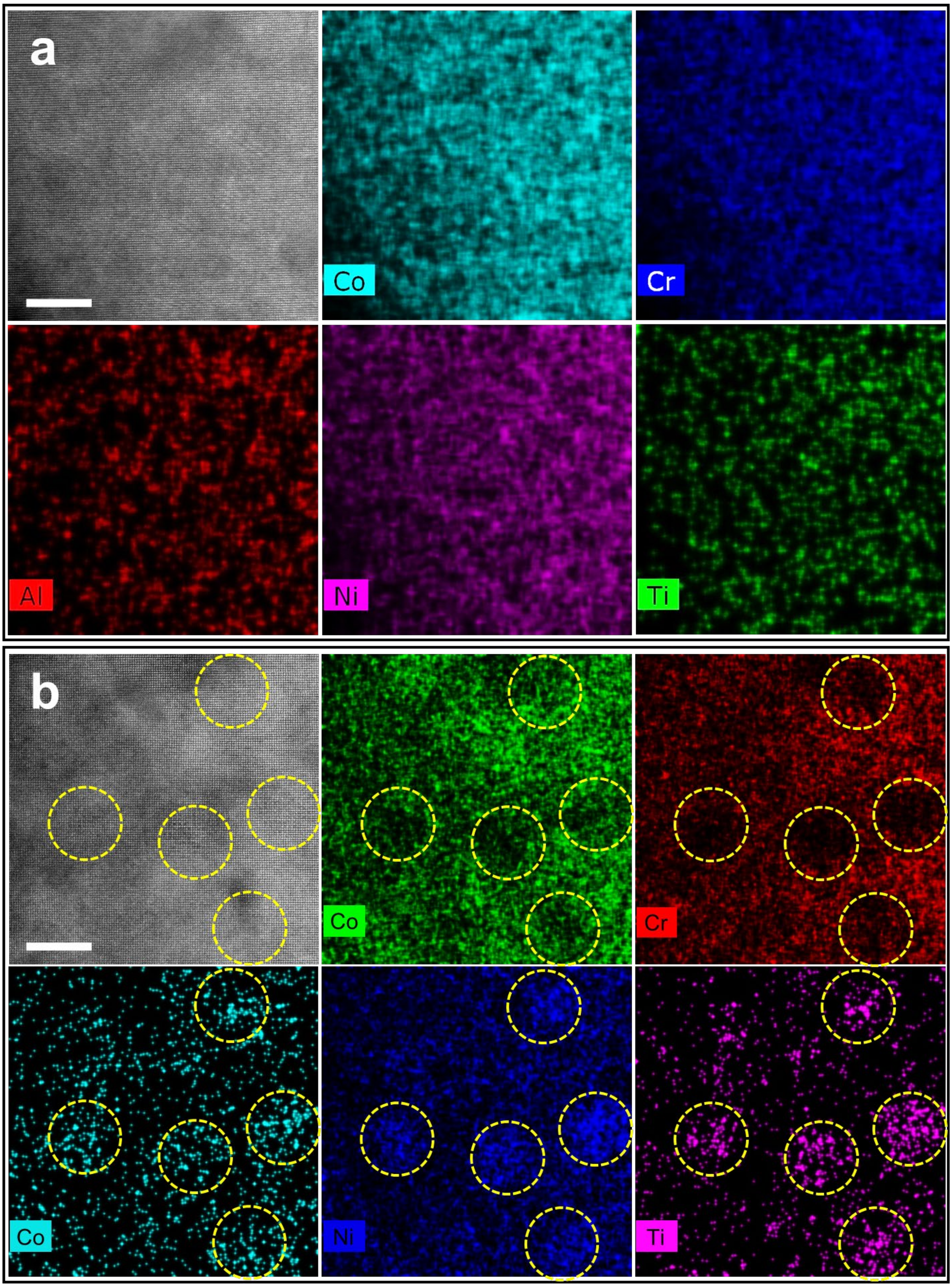


**Supplementary Figure 4. Microstructure difference between CRA and CRAA alloys.** Atomic-resolution HAADF-STEM image taken from [001] and corresponding EDS maps of **(a)** CRA and **(b)** CRAA alloys, showing that all five elements homogeneously distributed in CRA alloy while high-density $L1_2$ particles (with an average diameter of 4.14±0.62 nm) are precipitated in CRAA alloy. The scale bars in **(a)** and **(b)** are both 5 nm.

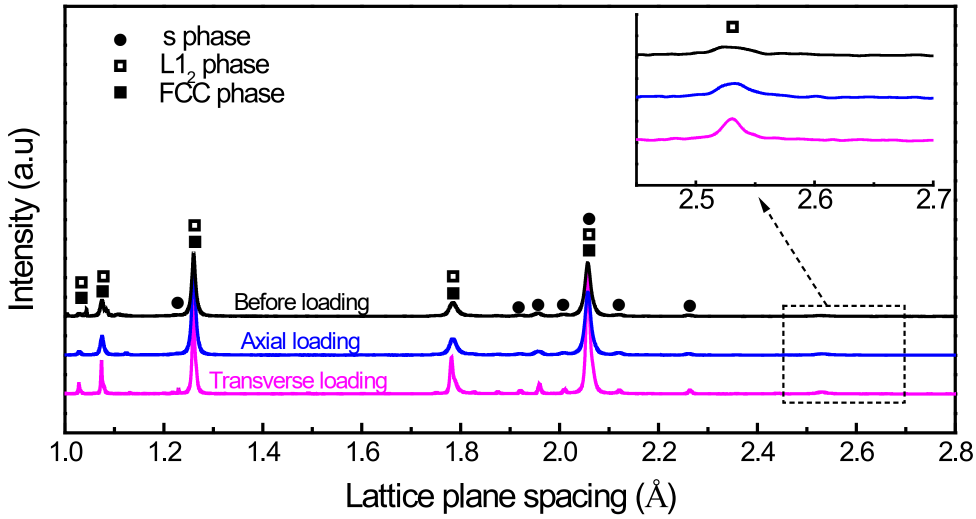


**Supplementary Figure 5. Synchrotron X-ray diffraction (SXRD) spectrums of the without loaded, axially loaded and transversely loaded CRAA samples.** It reveals that no phase transformation occurs during tensile process.

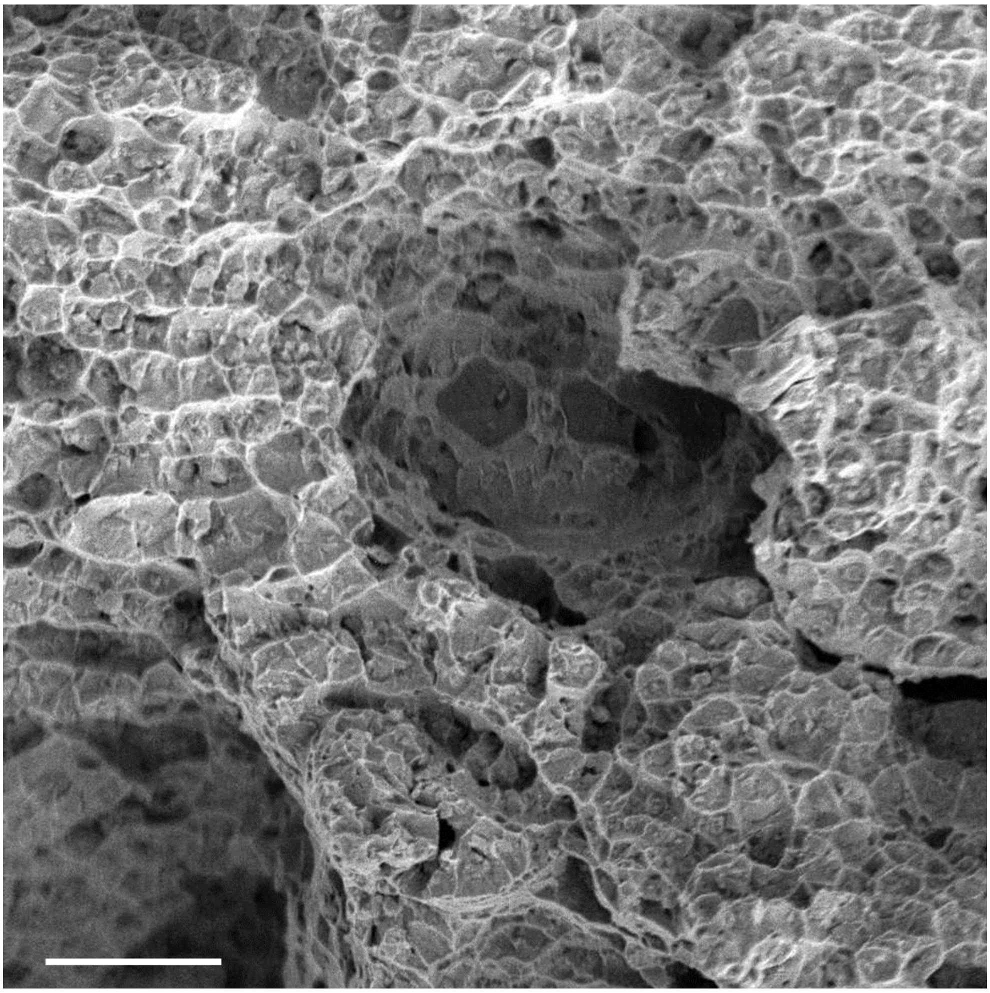

**Supplementary Figure 6. The fracture morphology of the CRAA alloy.** The SEM image shows obviously plastic deformation together with a micro-void coalescence fracture mode with fine dimples, indicating an excellent combination of ultra-high strength and good ductility. Scale bar, 5 μm.

## Supplementary References


1 Heslop, J. Wrought nickel-chromium heat-resisting alloys containing cobalt. *Cobalt* **24**, 128-134, (1964).

2 Liu, S. F., Wu, Y., Wang, H. T., Lin, W. T., Shang, Y. Y., Liu, J. B., An, K., Liu, X. J., Wang, H. & Lu, Z. P. Transformation-reinforced high-entropy alloys with superior mechanical properties via tailoring stacking fault energy. *Journal of Alloys and Compounds* **792**, 444-455, (2019).

3 Yang, Z. a., Xiao, Y. & Shi, C. The role of cobalt in the high temperature creep of $\gamma'$-strengthened nickel-based superalloys. *Materials Science and Engineering A* **101**, 65-73, (1988).

4 Yang, T., Zhao, Y. L., Tong, Y., Jiao, Z. B., Wei, J., Cai, J. X., Han, X. D., Chen, D., Hu, A., Kai, J. J., Lu, K., Liu, Y. & Liu, C. T. Multicomponent intermetallic nanoparticles and superb mechanical behaviors of complex alloys. *Science* **362**, 933-937, (2018).

5 Ardell, A. J. Precipitation hardening. *Metallurgical Transactions A* **16**, 2131-2165, (1985).

6 Zhao, Y. L., Yang, T., Tong, Y., Wang, J., Luan, J. H., Jiao, Z. B., Chen, D., Yang, Y., Hu, A., Liu, C. T. & Kai, J. J. Heterogeneous precipitation behavior and stacking-fault-mediated deformation in a CoCrNi-based medium-entropy alloy. *Acta Materialia* **138**, 72-82, (2017).

7 Pollock, T. M. & Argon, A. S. Creep resistance of CMSX-3 nickel base superalloy single crystals. *Acta Metallurgica Et Materialia* **40**, 1-30.

8 Gerold, V. & Pham, H.-M. Precipitation hardening by misfitting particles and its comparison with experiments. *Scripta Metallurgica* **13**, 0-898.

9 Raynor, D. & Silcock, J. M. Strengthening Mechanisms in $\gamma'$ Precipitating Alloys. *Metal Science Journal* **4**, 121-130, (1970).

10 Gardner, H., Pedrazzini, S., Douglas, J. O., De Lille, D., Moody, M. P. & Bagot, P. A. J. Atom Probe Tomography Investigations of Microstructural Evolution in an Aged Nickel Superalloy for Exhaust Applications. *Metallurgical and Materials Transactions A* **50**, 1862-1872, (2019).

11 Senkov, O. N. & Semiatin, S. L. Microstructure and properties of a refractory high-entropy alloy after cold working. *Journal of Alloys and Compounds* **649**, 1110-1123, (2015).

12 Schuh, B., Völker, B., Todt, J., Schell, N., Perrière, L., Li, J., Couzinié, J. P. & Hohenwarter, A. Thermodynamic instability of a nanocrystalline, single-phase TiZrNbHfTa alloy and its impact on the mechanical properties. *Acta Materialia* **142**, 201-212, (2018).

13 Shahmir, H., He, J., Lu, Z., Kawasaki, M. & Langdon, T. G. Effect of annealing on mechanical properties of a nanocrystalline CoCrFeNiMn high-entropy alloy processed by high-pressure torsion. *Materials Science and Engineering: A* **676**, 294-303, (2016).

14 Zheng, R., Chen, J., Xiao, W. & Ma, C. Microstructure and tensile properties of nanocrystalline (FeNiCoCu)1−xTixAlx high entropy alloys processed by high pressure torsion. *Intermetallics* **74**, 38-45, (2016).

15 Ming, K., Bi, X. & Wang, J. Precipitation strengthening of ductile Cr 15 Fe 20 Co 35 Ni 20 Mo 10 alloys. *Scripta Materialia* **137**, 88-93, (2017).

16 He, J. Y., Wang, H., Huang, H. L., Xu, X. D., Chen, M. W., Wu, Y., Liu, X. J., Nieh, T. G., An, K. & Lu, Z. P. A precipitation-hardened high-entropy alloy with outstanding tensile properties. *Acta Materialia* **102**, 187-196, (2016).

17 Huang, H., Wu, Y., He, J., Wang, H., Liu, X., An, K., Wu, W. & Lu, Z. Phase-Transformation Ductilization of Brittle High-Entropy Alloys via Metastability Engineering. *Adv Mater* **29**, (2017).

18 Moravcik, I., Cizek, J., Zapletal, J., Kovacova, Z., Vesely, J., Minarik, P., Kitzmantel, M., Neubauer, E. & Dlouhy, I. Microstructure and mechanical properties of Ni1,5Co1,5CrFeTi0,5 high entropy alloy fabricated by mechanical alloying and spark plasma sintering. *Materials & Design* **119**, 141-150, (2017).

19 Fu, Z. Q., Jiang, L., Wardini, J. L., MacDonald, B. E., Wen, H. M., Xiong, W., Zhang, D. L., Zhou, Y. Z., Rupert, T. J., Chen, W. P. & Lavernia, E. J. A high-entropy alloy with hierarchical nanoprecipitates and ultrahigh strength. *Sci. Adv.* **4**, 8, (2018).

20 Liang, Y. J., Wang, L., Wen, Y., Cheng, B., Wu, Q., Cao, T., Xiao, Q., Xue, Y., Sha, G., Wang, Y., Ren, Y., Li, X., Wang, L., Wang, F. & Cai, H. High-content ductile coherent nanoprecipitates achieve ultrastrong high-entropy alloys. *Nat Commun* **9**, 4063, (2018).

21 Su, J., Raabe, D. & Li, Z. Hierarchical microstructure design to tune the mechanical behavior of an interstitial TRIP-TWIP high-entropy alloy. *Acta Materialia* **163**, 40-54, (2019).